Accurate Computation of the Radiation from Simple Antennas Using the Finite-Difference Time-Domain Method

JAMES G. MALONEY, STUDENT MEMBER, IEEE, GLENN S. SMITH, FELLOW, IEEE, AND WAYMOND R. SCOTT, JR., MEMBER, IEEE

Abstract—**Two antennas are considered, a cylindrical monopole and a conical monopole. Both are driven through an image plane from a coaxial transmission line. Each of these antennas corresponds to a well-posed theoretical electromagnetic boundary value problem and a realizable experimental model. These antennas are analyzed by a straightforward application of the finite-difference time-domain (FD-TD) method. The computed results for these antennas, for both the time domain and the frequency domain, are shown to be in excellent agreement with accurate experimental measurements. The graphical displays presented for the transient near-zone and far-zone radiation from these antennas provide physical insight into the radiation process.**

I. INTRODUCTION

SIMPLE RADIATORS such as the cylindrical monopole/dipole, biconical monopole/dipole, circular loop and open-ended waveguides have received considerable attention in the literature. These radiators are generally the first ones discussed in a course on antenna analysis. They are analyzed using Maxwell's equations, and the theoretical results, such as input impedance, field patterns, etc., are compared with experimental measurements. When good agreement is obtained for the theory and experiment, one is presented with a convincing argument for the validity and usefulness of the theory.

The theoretical analysis of these radiators is generally carried out in two steps: the formulation of a theoretical model which corresponds, as closely as possible, to the actual antenna, and the analysis of the model using a particular mathematical technique. The theoretical model used for the antenna usually involves approximations introduced to simplify the analysis. For example, for the cylindrical dipole antenna an idealized source is often used, the so-called "delta-function generator" [1]. This source does not correspond to any realizable experimental model. Often the equations involved in the analysis of the antenna are also approximate. For example, for the cylindrical dipole antenna an approximate integral equation (thin-wire approximation) is often substituted for the exact integral equation. Approximations, like those mentioned above, lead to discrepancies between theoretical and experimental results, and it is often difficult to quantitatively ascertain the effects of the different approximations.

Accurate models and accurate theoretical analyses have been used with these simple radiators, but their complexity often puts them beyond the grasp of one first undertaking antenna analysis. For example, the cylindrical monopole can be modeled with the geometry shown in Fig. 1, which corresponds very closely to the arrangement used in experimental measurements. A rigorous mathematical analysis for this geometry due to Morris involves a coupled pair of singular integral equations whose numerical solution is a formidable task [2], [3].

The time-dependent Maxwell's differential equations can be represented by a set of difference equations that can be solved numerically using a digital computer. This procedure is often referred to as the finite-difference time-domain (FD-TD or TD-FD) method. This approach to solving electromagnetic problems is straightforward and easily understood by one first undertaking antenna analysis. In addition, the method is easily adapted to complex geometries, so simplified theoretical models are not required. The FD-TD method has been applied to problems of scattering and interaction, such as scattering from spheres, plates, etc., and the penetration of a field into the interior of cylindrical shields [4]–[9]. However, there has been little application of the method to antenna problems (driven).

In this paper the FD-TD method is used to analyze two radiators, a cylindrical monopole and a conical monopole, both antennas are driven through an image plane from a coaxial line. There are three objectives: first, to describe the formulation of theoretical models for these antennas that correspond to realizable experimental configurations; second, to apply the FD-TD method to these models and show that the theoretical results (time-domain and frequency-domain) are in excellent agreement with accurate experimental measurements; and third, to use the FD-TD results to describe the transient radiation from these antennas. The graphical displays presented

Manuscript received January 19, 1989; revised August 28, 1989. This work was supported in part by the Joint Services Electronics Program under Contracts DAAG29-84-K-0024 and DAAL03-87-K-0059.

The authors are with the School of Electrical Engineering, Georgia Institute of Technology, Atlanta, GA 30332.

IEEE Log Number 9035917.

0018-926X/90/0700-1059$01.00

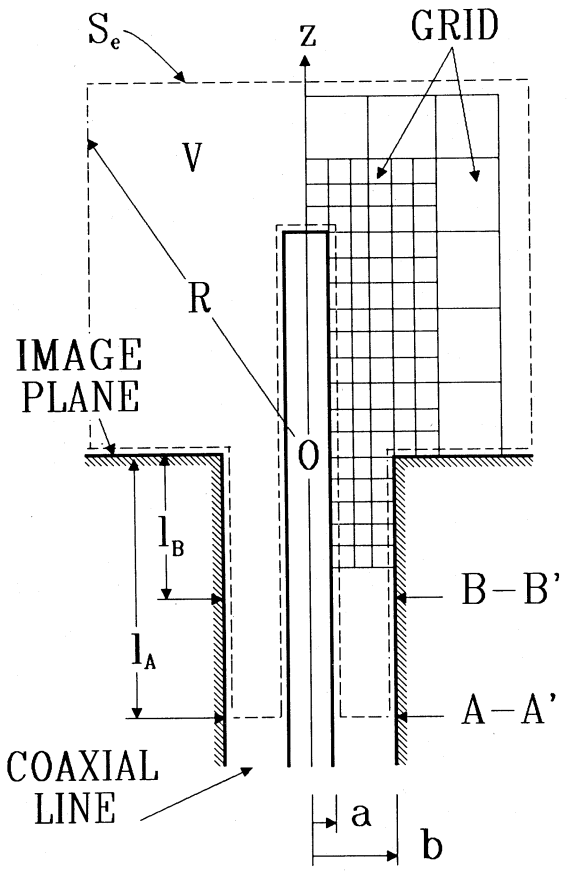

Fig. 1. Geometry for the electromagnetic boundary value problem —monopole antenna fed through an image plane from a coaxial transmission line.

for the transient radiation provide physical insight into the radiation process.

II. Formulation of the Antenna Problem

The theoretical analysis for an antenna begins with the formulation of a well-posed electromagnetic boundary value problem; ideally, one that closely corresponds to an actual antenna/experimental model. Fig. 1 shows the geometry for a monopole antenna fed through an image plane from a coaxial transmission line. This geometry will be used to illustrate the boundary value problem; other simple radiators can be handled in a similar manner.

The volume of free space V in which the electromagnetic field is to be determined surrounds the antenna and extends into the coaxial line to the depth $z = -l_A$. The boundary surface of the region is indicated by the dashed line in Fig. 1. All conductors are assumed perfect, and the field is to be determined within V for times $0 < t \leq t_0$.

To obtain a unique solution to Maxwell's equations within V for times $0 < t \leq t_0$, we must specify $\vec{\mathcal{E}}$ and $\vec{\mathcal{H}}$ within V at time $t = 0$. In addition, $\hat{n} \times \vec{\mathcal{E}}$ or $\hat{n} \times \vec{\mathcal{H}}$ must be specified on the boundary surface of V for all times $0 < t \leq t_0$ [10].

We will assume that the electromagnetic field ($\vec{\mathcal{E}}$ and $\vec{\mathcal{H}}$) is zero within V at time $t = 0$. On the cross section of the coaxial line at $A-A'$ ($z = -l_A$), the tangential component of the incident electric field ($-\hat{z} \times \vec{\mathcal{E}}^i$) is specified for times $0 < t \leq t_0$. Now this will be the only electric field at this cross section if we choose $2l_A > ct_0$, because the field reflected from the end of the line will not reach this cross section during the observation time. Since we have perfect conductors, $\hat{n} \times \vec{\mathcal{E}} = 0$ on the surface of the coaxial line, antenna and ground plane. The minimum distance to the surface S_e that surrounds the antenna above the image plane is $R_{\min}$. When $R_{\min} > ct_0 - l_A$, the electromagnetic field ($\hat{n} \times \vec{\mathcal{E}}$ and $\hat{n} \times \vec{\mathcal{H}}$) will be zero on the surface S_e for all observation times. A review of the above specifications shows that all the requirements have been met for obtaining a unique solution to Maxwell's equations within the volume V for times $0 < t \leq t_0$.

The dimensions of the coaxial transmission line, a and b, are chosen so that only a transverse electromagnetic (TEM) mode can propagate within the line for the signals of interest. Thus, on the cross section $A-A'$ the incident electric field is

$$\vec{\mathcal{E}}^i(t) = \frac{\mathcal{V}^i(t)}{\ln(b/a)r}\hat{r}. \tag{1}$$

The radiators considered represent two-dimensional electromagnetic problems. For example, the radiator in Fig. 1 is rotationally symmetric and is excited by a rotationally symmetric source. Therefore, the electromagnetic field is independent of the cylindrical coordinate ϕ, and Maxwell's equations can be expressed as two independent sets: one that involves only the components $\mathcal{E}_\phi$, $\mathcal{H}_r$, $\mathcal{H}_z$, the transverse electric (TE) field; and one that involves only the components $\mathcal{E}_r$, $\mathcal{E}_z$, $\mathcal{H}_\phi$, the transverse magnetic (TM) field. Since the excitation for the antenna in Fig. 1 is a TEM mode, which has only the field components $\mathcal{E}_r$, $\mathcal{H}_\phi$, only the rotationally symmetric TM modes are excited. The relevant Maxwell's equations are then

$$\frac{\partial \mathcal{E}_r}{\partial z} - \frac{\partial \mathcal{E}_z}{\partial r} = -\mu_0 \frac{\partial \mathcal{H}_\phi}{\partial t}, \tag{2a}$$

$$-\frac{\partial \mathcal{H}_\phi}{\partial z} = \epsilon_0 \frac{\partial \mathcal{E}_r}{\partial t}, \tag{2b}$$

$$\frac{1}{r}\frac{\partial (r\mathcal{H}_\phi)}{\partial r} = \epsilon_0 \frac{\partial \mathcal{E}_z}{\partial t}. \tag{2c}$$

In the FD-TD formulation both space and time are discretized. For the spatial increments Δr and Δz, and the time increment Δt the notation is

$$\mathcal{E}_z(r, z, t) = \mathcal{E}_z(i\Delta r, j\Delta z, n\Delta t) = \mathcal{E}_z^n(i, j).$$

For Yee's method of discretization, components of $\vec{\mathcal{E}}$ and $\vec{\mathcal{H}}$ are evaluated at interleaved spatial grid points and interleaved time steps [4]. The spatial grid points for the cylindrical system (r, ϕ, z) and the field components evaluated at these points are shown in Fig. 2. The Maxwell's equations (2) after discretization are

$$\mathcal{H}_\phi^{n+0.5}(i, j) = \mathcal{H}_\phi^{n-0.5}(i, j) + \frac{\Delta t}{\mu_0 \Delta r}[\mathcal{E}_z^n(i + 0.5, j) - \mathcal{E}_z^n(i - 0.5, j)] - \frac{\Delta t}{\mu_0 \Delta z}[\mathcal{E}_r^n(i, j + 0.5) - \mathcal{E}_r^n(i, j - 0.5)], \tag{3a}$$

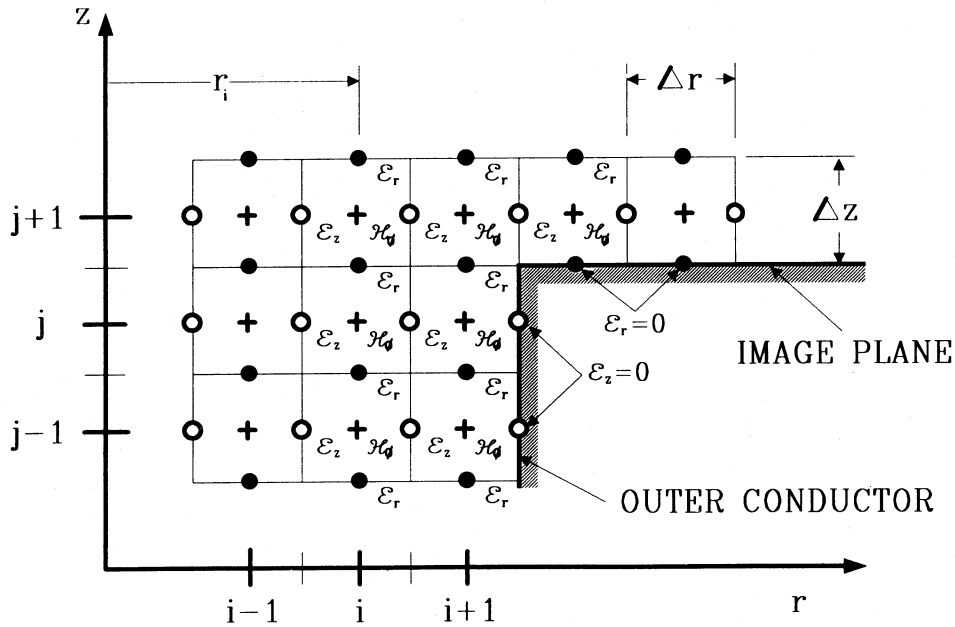

Fig. 2. Spatial grid and field components for the two-dimensional problem with cylindrical symmetry.

$$\mathcal{E}_r^{n+1}(i, j-0.5) = \mathcal{E}_r^{n}(i, j-0.5) - \frac{\Delta t}{\epsilon_0 \Delta z} \cdot [\mathcal{H}_\phi^{n+0.5}(i, j) - \mathcal{H}_\phi^{n+0.5}(i, j-1)], \quad (3b)$$

$$\mathcal{E}_z^{n+1}(i+0.5, j) = \mathcal{E}_z^{n}(i+0.5, j) + \frac{\Delta t}{\epsilon_0 \Delta r} \frac{1}{r_{i+0.5}} \cdot [r_{i+1}\mathcal{H}_\phi^{n+0.5}(i+1, j) - r_i \mathcal{H}_\phi^{n+0.5}(i, j)]. \quad (3c)$$

Note that the grid in Fig. 2 is arranged so that the electric field component tangential to the surface of a perfect conductor is evaluated at the surface. With the tangential electric field $\vec{\mathcal{E}}_r$ specified at the boundary $A - A'$, these equations (3a)–(3c) are used in a time-stepping procedure to determine the electromagnetic field in the volume V for times $0 < t \leq t_0$.

In a practical implementation an absorbing boundary condition is used at the surface S_e; this allows the observation period to be extended beyond $t = t_0$. Various **approximately** absorbing boundary conditions have been proposed; the one used here is due to Merewether [5]. In this approach the field near the boundary is assumed to have the functional form $f(t - R/c)/R$, and the tangential component of the electric field on the surface S_e is computed from local values within V by interpolation. The TEM field within the coaxial line has a known functional form $f(t - z/c)$; thus, an **exactly** absorbing boundary condition can be constructed within the line. In this procedure the incident field is additively injected at a plane $z = -l$, and the absorbing boundary condition, placed at $z = -(l + \Delta z)$, exactly absorbs the field of a TEM mode propagating in the $-z$ direction. This allows the cross section at which the incident field is specified to be moved closer to the ground plane; namely, in Fig. 1 $B - B'$ ($z = -l_B$) is used instead of $A - A'$ ($z = -l_A$).[1] This reduces both the time required for observation and the size of the grid.

[1]The plane $B - B'$ must be chosen so that all the evanescent TM modes present at $z = 0$ are insignificant at $z = -l_B$, typically $l_B = 3(b - a)$.

The spatial and temporal increments (Δr, Δz, and Δt) are chosen to satisfy the "domain of dependence condition" or "Courant–Friedrichs–Lewy condition" [11]:

$$c\Delta t \leq \sqrt{\frac{\Delta r^2 \Delta z^2}{\Delta r^2 + \Delta z^2}}. \quad (4)$$

In this work two spatial grid spacings are used: a fine spacing ($\Delta r_1 \approx \Delta z_1$) within the coaxial line and close to the antenna where the field is varying rapidly with spatial position, and a course grid ($\Delta r_2 = (3\text{–}5)\Delta r_1$, $\Delta z_2 = (3\text{–}5)\Delta z_1$) in the remainder of the space. The use of the dual grid reduces computer storage. Note, when (4) is satisfied for the fine grid it is automatically satisfied for the course grid. In the examples that follow

$$c\Delta t = \frac{\min(\Delta r_1, \Delta z_1)}{2}, \quad (5)$$

and the increments Δr_1, Δz_1 are chosen small enough to resolve the spatial variation of the field.

III. Comparison of Theoretical and Experimental Results

In this section the FD–TD method is used to analyze two antennas: a cylindrical monopole and a conical monopole, both are driven through an image plane from a coaxial transmission line. The theoretical models for each of these radiators fit the formulation presented in Section II and correspond closely to realizable experimental configurations.

A. Cylindrical Monopole

The cylindrical monopole antenna shown in Fig. 3(a) has been studied extensively both theoretically and experimentally; it is one of the canonical problems in antenna analysis. Various approximations have been used to make the theoretical analysis tractable, such as assuming a TEM field in the coaxial aperture at the image plane ($z = 0$) [12], [13]. An

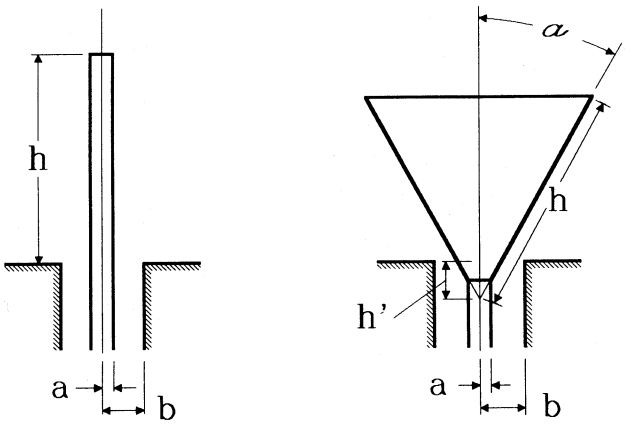

Fig. 3. Dimensions for the antenna models. (a) Cylindrical monopole. (b) Conical monopole.

accurate analysis of the correct boundary value problem, the one that corresponds to the experimental model, was carried out by Morris in 1980 and verified by accurate experimental measurements [2], [3]. Here a straightforward application of the FD-TD method to this antenna will be shown to produce results of comparable accuracy.

The parameters that describe the monopole antenna are the height h and the radii of the conductors of the coaxial line a and b. For the results shown in Figs. 4–7 $b/a = 2.30$, which corresponds to a characteristic impedance of 50 Ω for the coaxial line. Two grid spacings were used, as in Fig. 1: $\Delta r_1 = (b - a)/4$, $\Delta z_1 = h/203$; and $\Delta r_2 = 3\Delta r_1$, $\Delta z_2 = 3\Delta z_1$.

The cylindrical monopole was first studied for a Gaussian pulse excitation; the incident electric field in the transmission line at reference plane $A - A'$ being (1) with

$$\mathcal{V}^i(t) = V_0 \exp(-t^2/2\tau_p^2). \tag{6}$$

The antenna is characterized by the time $\tau_a = h/c$; this is the time required for light to travel its length. For the results shown in Figs. 4–7 the ratio of the characteristic time for the Gaussian pulse τ_p to the characteristic time for the antenna τ_a is $\tau_p/\tau_a = 8.04 \times 10^{-2}$.[2]

Fig. 4 shows the surface charge density on the coaxial line and antenna as a function of the normalized position z/h and the normalized time t/τ_a. This is the surface charge density on the inner conductor of the coaxial line for $-1.0 \le z/h < 0.0$ and on the antenna for $0.0 \le z/h \le 1.0$. This bounce diagram clearly shows that the pulse travels up the coaxial line until it reaches the aperture ($z/h \approx 0.0$, $t/\tau_a \approx 1.0$; A in Fig. 4). At this point a portion of the pulse is reflected back into the line, and the remainder emerges on the antenna. The pulse is next reflected at the end of the antenna ($z/h \approx 1.0$, $t/\tau_a \approx 2.0$; B); then, it travels down to the aperture ($z/h \approx 0.0$, $t/\tau_a \approx 3.0$; C) where it is partially reflected and enters the coaxial line. This process is then repeated.

[2]The pulse duration was chosen short enough to resolve the reflections from different points on the antenna. However, the pulse duration is not so short that it excites propagating TM modes (other than the TEM mode) in the coaxial line. At the cutoff frequency for the lowest mode, the TM_{01}, the spectrum of the pulse is reduced by the factor $\approx 3 \times 10^{-32}$ from its maximum.

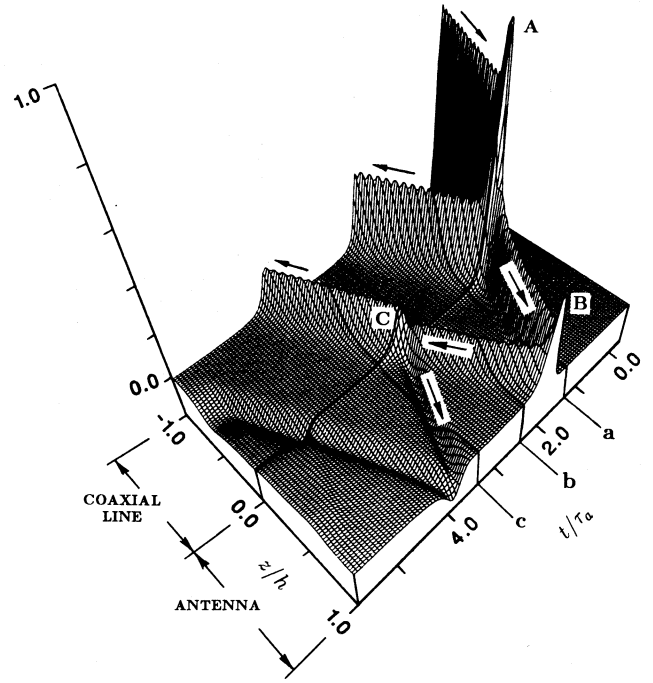

Fig. 4. Normalized surface charge density on the cylindrical monopole antenna as a function of the normalized position z/h and the normalized time t/τ_a: $b/a = 2.30$, $h/a = 65.8$, and $\tau_p/\tau_a = 8.04 \times 10^{-2}$.

The peaks at the points A and B are the result of the singularities in the charge density that occur at the sharp edges of the structure. The concentration of charge at A is produced by the singularity at the edge of the outer conductor of the coaxial line, while the spike at B is the singularity at the edge on the top of the antenna.

The electric field surrounding the monopole antenna is displayed on a gray scale in Fig. 5 for three times. Graphs of the surface charge density on the antenna are below each plot; these correspond to the slices marked a, b, and c in Fig. 4. The spacing between the conductors of the coaxial line is expanded in these plots to clarify the presentation.

In Fig. 5(a) the pulse has been reflected at the aperture and is traveling out along the antenna. The spherical wavefront centered on the aperture (W_1 in Fig. 5(a)) is attached to packets of charge on the antenna and image plane. A second wavefront (W_2) is produced when this pulse is reflected at the end of the antenna. This spherical wavefront, centered on the end of the antenna, is clearly shown in Fig. 5(b). The pulse, after reflection from the end, travels down the antenna, eventually being partially reflected at the aperture and entering the coaxial line. A third spherical wavefront (W_3), centered at the aperture, is produced on this reflection, Fig. 5(c). The effect the image plane has on the wavefront W_2 is easily understood when the dipole configuration of the antenna is viewed, Fig. 6. The wavefront W_{2R}, the reflection of wavefront W_2 at the image plane, is seen to be the same as the wavefront radiated from the opposite end of the dipole.

For times beyond those shown in Fig. 5, the pulse travels along the antenna alternately being reflected at the end and coaxial aperture and decreasing in amplitude. Eventually there is no charge on the antenna, and the radiation ceases. At each reflection a wavefront similar to one in Fig. 5 is produced;

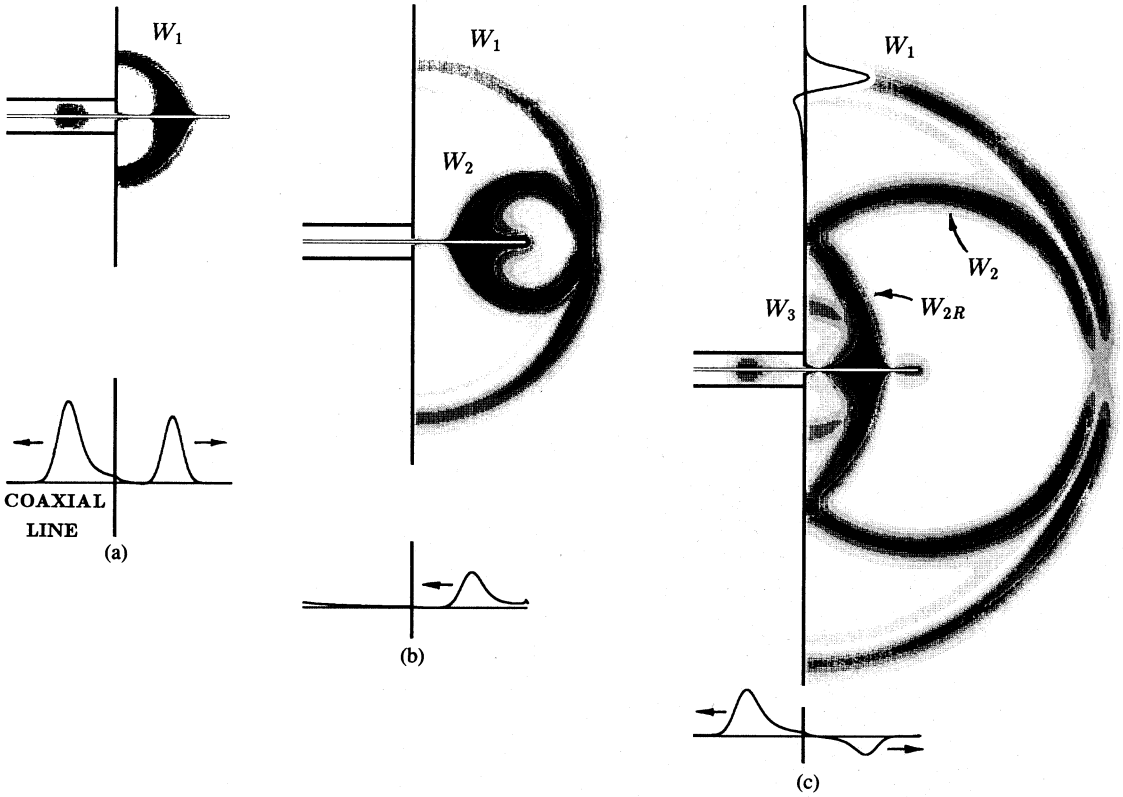

Fig. 5. Radiation of a Gaussian pulse from a cylindrical monopole antenna. Gray scale plots show the magnitude of the electric field, the line drawings show the surface charge density on the antenna. $b/a = 2.30$, $h/a = 65.8$, and $\tau_p/\tau_a = 8.04 \times 10^{-2}$.

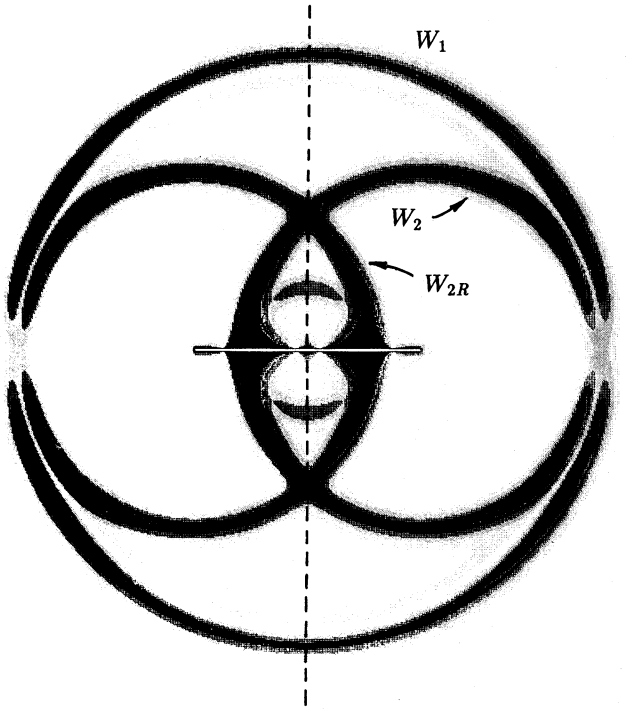

Fig. 6. Dipole configuration corresponding to Fig. 5(c).

for example, the next waveform W_4, which is similar to W_2, is produced when the pulse traveling up the antenna is again reflected at the end.

To complete the description of the radiation from this antenna, the electric field in the far zone will be determined. This is accomplished by using the electromagnetic form of Huygens' principle to continue the FD–TD results to the far zone. In particular, the electric field $\vec{\mathcal{E}}^r$ in the far zone is

$$\vec{\mathcal{E}}^r(\vec{r}, t) = \frac{\mu_0}{4\pi r} \oint\!\!\!\oint_S \{\hat{r} \times \hat{r} \times \frac{\partial}{\partial t'}[\hat{n} \times \vec{\mathcal{H}}(\vec{r}', t')] - \frac{1}{\zeta_0}\hat{r} \times \frac{\partial}{\partial t'}[\hat{n} \times \vec{\mathcal{E}}(\vec{r}', t')]\}\, dS|_{t'=t-|\vec{r}-\vec{r}'|/c}, \quad (7)$$

where $\vec{r}$ locates the point in the far zone, $\vec{r}'$ locates the point on the surface S surrounding the antenna, and the outward normal to this surface is $\hat{n}$.[3]

The far-zone electric field $\mathcal{E}_\theta^r$ for the cylindrical monopole antenna is shown in Fig. 7. The surface used in (7) for these calculations was the cylindrical boundary separating the fine and coarse grids in Fig. 1. Each trace in this figure shows the electric field at a fixed polar angle θ as a function of the normalized time t/τ_a. On these graphs the origin for the time, $\tau/\tau_a = 0$, and the amplitude for the field were selected to clarify the presentation. Notice that wavefronts from the same point on the antenna are always separated by a time interval which is a multiple of $2\tau_a$, the round-trip transit time for the pulse on the antenna. For example, wavefronts W_1 and W_3, which are centered on the drive point, are separated by the time $2\tau_a$, as are wavefronts W_2 and W_4, which are centered on the end. However, the relative position of the wavefront pairs, such as W_1, W_3 and W_2, W_4, changes with the viewing angle θ. For example, at $\theta = 90°$ the wavefronts W_1, W_2,

[3]The frequency domain counterpart to this formula is presented in the literature [14], [15]. Equation (7) is obtained by specializing this formula to the far zone and then taking the inverse Fourier transform.

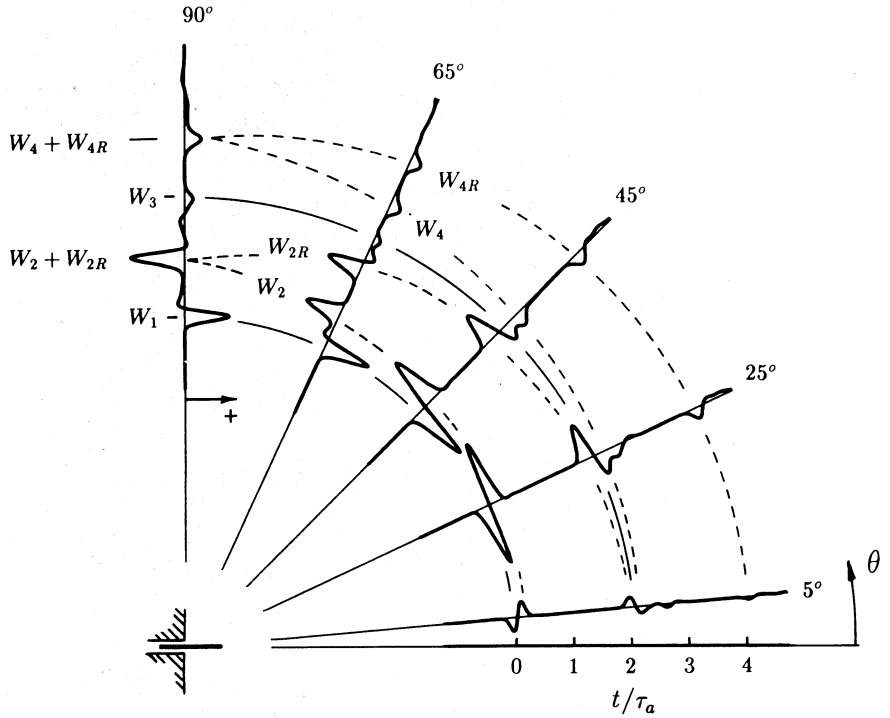

Fig. 7. Radiation of a Gaussian pulse from a cylindrical monopole antenna. Each trace shows the far-zone electric field $\mathcal{E}'_\theta$ at a fixed polar angle θ as a function of the normalized time t/τ_a. $b/a = 2.30$, $h/a = 65.8$, and $\tau_p/\tau_a = 8.04 \times 10^{-2}$.

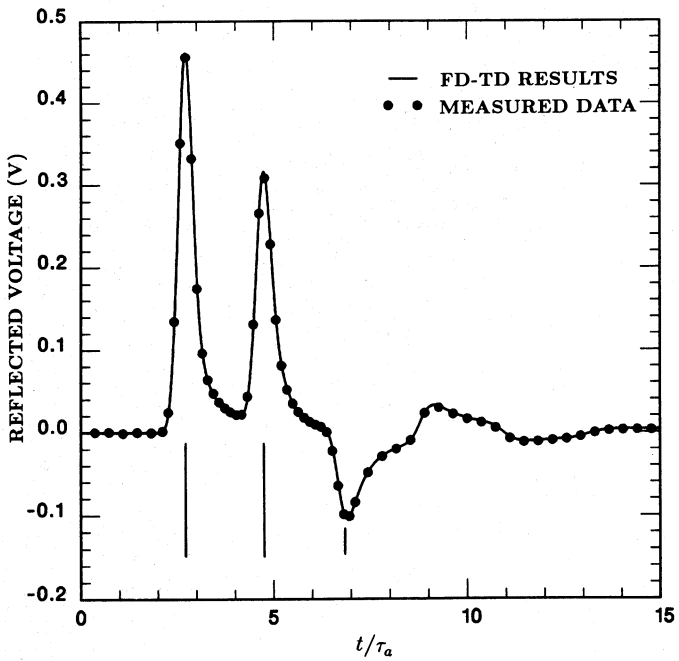

Fig. 8. Comparison of the theoretical (FD-TD) and the measured reflected voltages in the coaxial line for a cylindrical monopole antenna excited by a 1 V Gaussian pulse: $b/a = 2.30$, $h/a = 32.8$, and $\tau_p/\tau_a = 1.61 \times 10^{-1}$.

W_3 and W_4 are all separated, but at $\theta = 5°$ W_1 and W_2 are superposed as are W_3 and W_4. Of course, the far zone field off the end of the antenna is zero ($\theta = 0°$).

An experimental model was constructed for the cylindrical monopole antenna with the dimensions $b/a = 2.30$, $h/a = 32.8$. This model was mounted on an aluminum image plane (120 × 155 cm) that was surrounded by absorbing material to reduce reflections. The input reflection coefficient for this antenna was measured at a number of frequencies (50 MHz $\leq f \leq$ 18 GHz) using a Hewlett Packard Model 8409C Automated Network Analyzer. These data were then used with a fast Fourier transform to obtain the response of the antenna to a Gaussian pulse (6).

In Fig. 8 the reflected voltage measured in the coaxial line (dots) is compared with results computed by the FD–TD method (solid line) for a Gaussian pulse with $\tau_p/\tau_a = 1.61 \times 10^{-1}$. This is the reflected voltage at the plane $B - B'$ in Fig. 1 where only the TEM mode is present. The agreement between the two sets of data is excellent. Note that the peaks in the reflected voltage are spaced by about the round-trip transit time for the pulse on the antenna, $t/\tau_a = 2.0$.

As a second test, the FD–TD method was used to compute the response of a monopole excited by the signal

$$\mathcal{V}_i(t) = V_0 r(t) \sin(\omega t). \tag{8}$$

Here $r(t)$ is a ramp function which goes from 0 at time $t = 0$ to 1.0 at time $t = \tau_r$; τ_r is chosen to be several cycles of the sinusoid. The long-time response to this signal is approximately monochromatic and can be compared with frequency domain measurements.[4] The steady state sinusoidal voltage at the reference plane $B - B'$ in Fig. 1 is used to determine the reflection coefficient for the antenna, and this, in turn, determines the input admittance.

The geometry chosen corresponds to an antenna measured by Cooper: $b/a = 3.00$; $a/\lambda = 7.02 \times 10^{-3}$ [16]. The end of this antenna is hemispherical; it was modeled by six dis-

[4]The monochromatic case could be obtained by Fourier transforming a pulse response. This was not done, because the objective of this paper is to illustrate the direct use of the FD–TD method. For a single frequency the use of the Fourier transform with the FD–TD pulse response may also be less efficient, since the higher frequencies necessary in the pulse would require finer discretization in time and space.

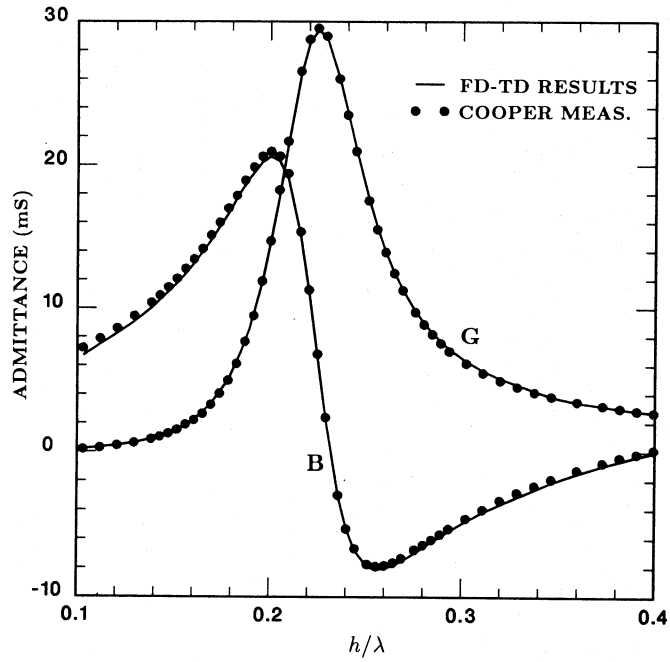

Fig. 9. Comparison of the theoretical (FD-TD) and the measured input admittances, $Y = G + jB$, for a cylindrical monopole antenna with a hemispherical end: $b/a = 3.00$, $a/\lambda = 7.02 \times 10^{-3}$.

crete steps in the FD-TD grid. In Fig. 9 the FD-TD results (solid line) are compared with Cooper's data (dots) for the input admittance measured for a range of lengths surrounding the first resonance of the antenna, $0.1 \leq h/\lambda \leq 0.4$. The agreement is very good, particularly when one considers that Cooper estimates the error bound on his data to be 5%.

B. Conical Monopole

The theoretical model usually used for the conical monopole antenna is a vertical, solid cone over an image plane. This structure is analyzed by expanding the electromagnetic field in spherical models [17], [18]. At the drive point of the antenna, the vertex of the cone, the input impedance is determined from the outwardly propagating and reflected TEM spherical waves. This theoretical model is only an approximation to the usual experimental model, a cone fed through an image plane by a coaxial transmission line as in Fig. 3(b). Thus, this modal analysis cannot produce results that are in extremely good agreement with experiment.

Here we use the FD-TD method to study the electromagnetic characteristics of the conical monopole antenna in Fig. 3(b). This antenna is described by the following parameters: b/a, h/a, h'/h and the half angle of the cone α. The antenna is characterized by a time $\tau_a = h/c$; this is the time required for light to travel over the slant height of the cone.

The grid spacings for the FD-TD method were essentially the same as those used with the cylindrical monopole. The side of the cone was handled by setting $\mathcal{E}_r$ and $\mathcal{E}_z$ equal to zero at all grid points inside the cone.

Fig. 10 shows the response of a conical monopole to a Gaussian pulse; the electric field in the transmission line being (1) with $\mathcal{V}^i(t)$ given by (6). The ratio of characteristic times is $\tau_p/\tau_a = 3.44 \times 10^{-2}$, and the other parameters for the antenna are $b/a = 2.30$, $h/a = 1.54 \times 10^2$, $h'/h = 1.34 \times 10^{-2}$ and $\alpha = 30°$. The electric field in the space surrounding the antenna is displayed on a gray scale, and the surface charge density on the antenna is shown below each plot. Again the spacing between the conductors of the coaxial line is expanded to clarify the presentation.

In Fig. 10(a) the Gaussian pulse has been reflected at the aperture and has moved out onto the antenna as the spherical wavefront W_1. When this pulse hits the top edge of the cone, Fig. 10(b), a second toroidal wavefront W_2, centered on the edge, is produced. Note that wavefront W_1 is attached to the packets of charge on the top of the cone and on the image plane, whereas waveform W_2 is attached to the packets of charge on the top and side of the cone.[5]

The charge packet on the side of the cone moves to the vertex, Fig. 10(c), where it eventually enters the coaxial line and is partially reflected to produce wavefront W_3, which is centered on the aperture, Fig. 10(d). The charge packet on the top of the cone, Figs. 10(b) and 10(c), travels across the top of the cone and produces a wavefront W_4 when it hits the opposite edge of the top, Fig. 10(d).

The far-zone electric field $\mathcal{E}_\theta^r$ for the conical monopole antenna is shown in Fig. 11. As for the cylindrical monopole, each trace is the electric field $\mathcal{E}_\theta^r$ at a fixed polar angle θ as a function of the normalized time t/τ_a. Notice that there are now two contributions from the wavefront W_1, marked W_1^A and W_1^B in Figs. 10 and 11. This is a result of the wavefront crossing itself on the top of the cone ($\theta = 0°$), as clearly seen in Figs. 10(c) and 10(d).

An experimental model was constructed for the conical monopole antenna with the dimensions $b/a = 2.30$, $h/a =$

[5]The division of the total field into specific wavefronts is somewhat arbitrary, since two or more of the wavefronts often overlap.

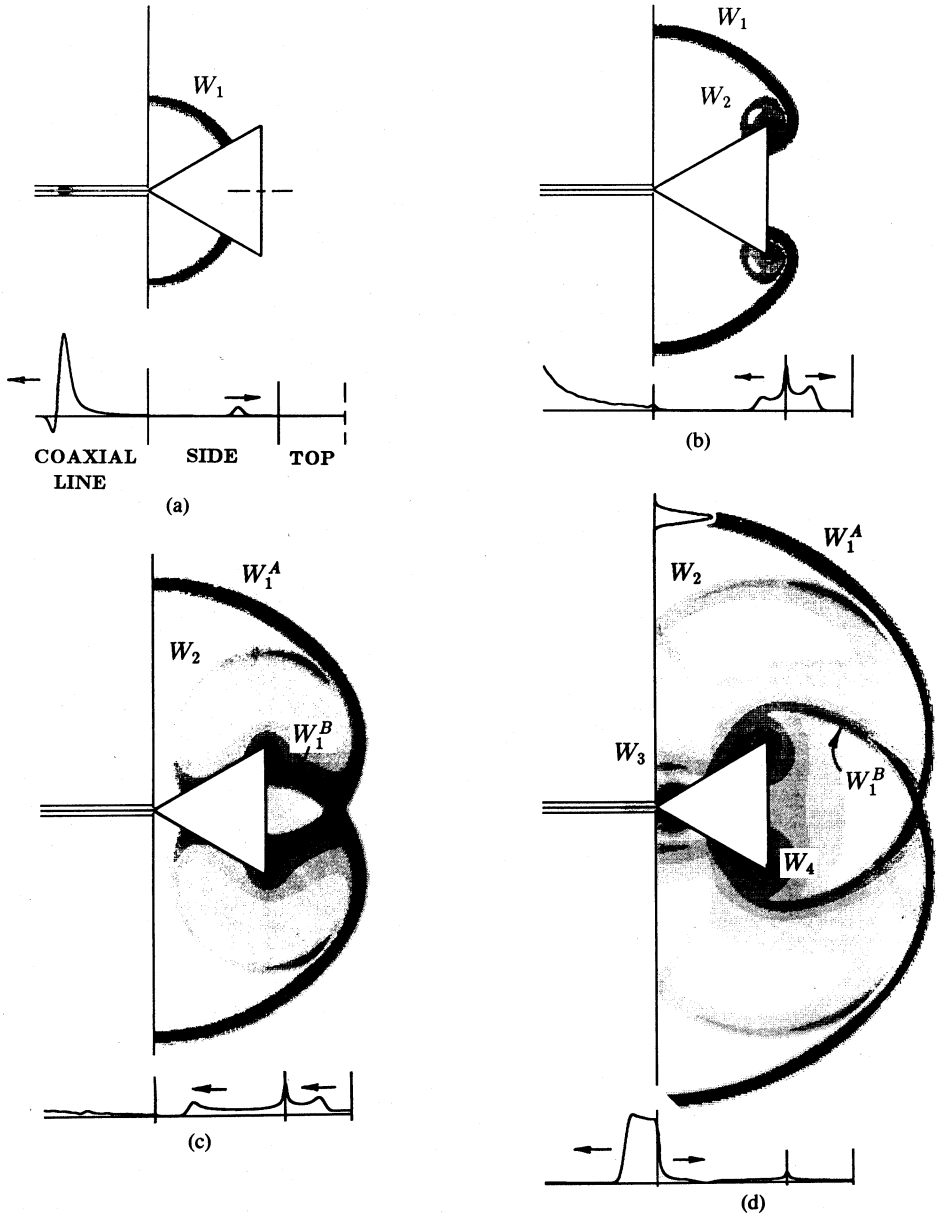

Fig. 10. Radiation of a Gaussian pulse from a conical monopole antenna. Gray scale plots show the magnitude of the electric field, the line drawings show the surface charge density on the antenna. $b/a = 2.30$, $h/a = 1.54 \times 10^2$, $h'/h = 1.34 \times 10^{-2}$, $\alpha = 30°$, and $\tau_p/\tau_a = 3.44 \times 10^{-2}$. Charge density is scaled in (b) and (c) by a factor of 15, and in (d) by a factor of 5.

23.1, $h'/h = 8.63 \times 10^{-2}$, and $\alpha = 30°$. The reflected voltage at the input of this antenna was measured in the same manner as for the cylindrical monopole. In Fig. 12 the measured reflected voltage (dots) is compared with results computed by the FD–TD method (solid line) for a Gaussian pulse with $\tau_p/\tau_a = 2.29 \times 10^{-1}$. The agreement between the two sets of data is excellent. The reflections due to the drive point and the near and far edges of the top are evident in this figure.

Note the small negative spike at the beginning of the waveform in Fig. 12. This is caused by the cone partially filling the coaxial aperture at $z = 0$, as in Fig. 3(b). This spike occurs whenever $h'/a > 1/\tan(\alpha)$. It is impressive that the FD–TD method handles this fine detail correctly.

IV. Summary and Conclusion

Two antennas were considered, a cylindrical monopole and a conical monopole, both are driven through an image plane from a coaxial transmission line. Each of these corresponds to a well-posed theoretical electromagnetic boundary value problem and a realizable experimental model. These antennas are structures of different complexity. The cylindrical monopole is a solid perfectly conducting structure with only right angle corners. The boundary surfaces of this antenna are at grid points where a tangential component of the electric field is set to zero. The conical monopole, however, involves corners of arbitrary angle (α) and a boundary surface (side) that does not pass through a specific set of grid points.

These antennas were analyzed by a straightforward application of the finite-difference time-domain method. The computed results are in excellent agreement with accurate experimental measurements. A survey of the literature for these antennas shows that no better results (in better agreement with measurement) have been obtained with analytical techniques or more involved numerical techniques.

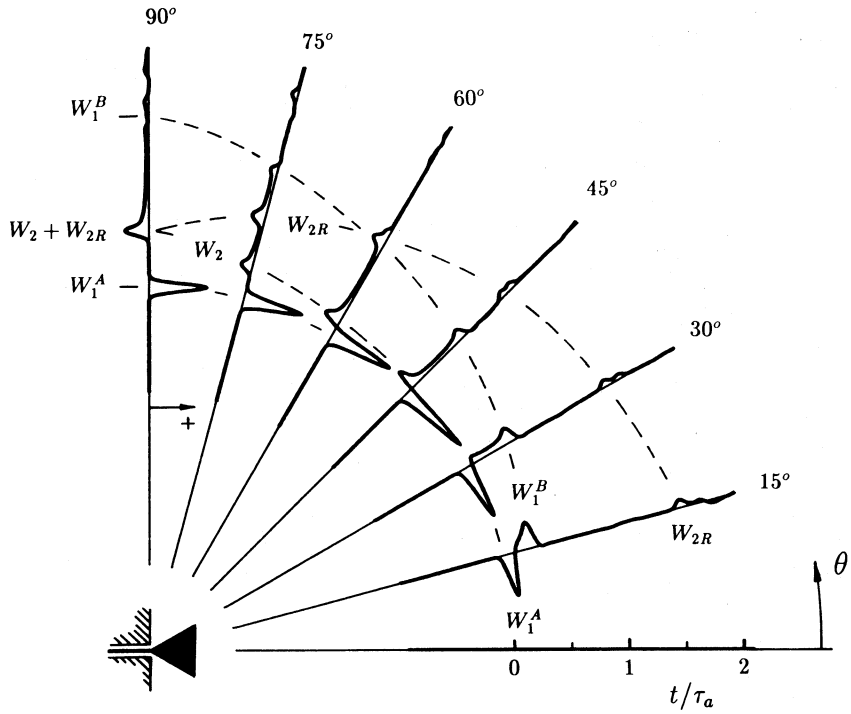

Fig. 11. Radiation of a Gaussian pulse from a conical monopole antenna. Each trace shows the far-zone electric field $\mathcal{E}_\theta^r$ at a fixed polar θ as a function of the normalized time t/τ_a. $b/a = 2.30$, $h/a = 1.54 \times 10^2$, $h'/h = 1.34 \times 10^{-2}$, $\alpha = 30°$, and $\tau_p/\tau_a = 3.44 \times 10^{-2}$.

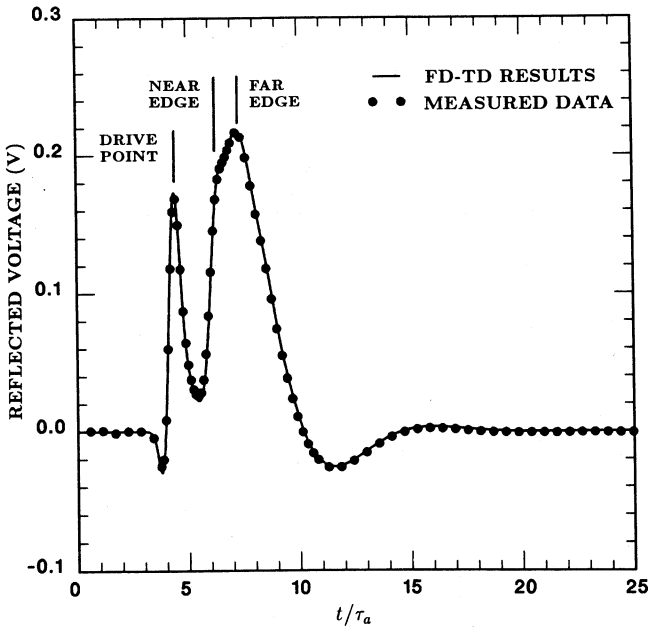

Fig. 12. Comparison of the theoretical (FD–TD) and the measured reflected voltages in the coaxial line for a conical monopole antenna excited by a 1 V Gaussian pulse: $b/a = 2.30$, $h/a = 23.1$, $h'/h = 8.63 \times 10^{-2}$, $\alpha = 30°$, and $\tau_p/\tau_a = 2.29 \times 10^{-1}$.

The graphical displays for the electromagnetic behavior of these antennas (the response to a pulse excitation) are presented in a manner that increases physical insight into the radiation process and is useful for instruction.

Acknowledgment

The authors would like to thank one of the reviewers for suggesting the inclusion of the graphs for the far-zone field, Figs. 7 and 11. These graphs enhance the description of the transient radiation.

References

[1] T. T. Wu and R. W. P. King, "Driving point and input admittance of linear antennas," *J. Appl. Phys.*, vol. 30, pp. 74–76, Jan. 1959.

[2] M. E. Morris, "Analysis of a finite length tubular monopole antenna driven by a coaxial line," Sandia Nat. Labs., Albuquerque, NM, Tech. Rep. SAND79-1557, May 1980.

[3] ——, "Precision admittance measurements of coaxially-driven monopole antennas—An experimental study of junction effects," Sandia Nat. Labs., Albuquerque, NM, Tech. Rep. SAND79-2047, May 1980.
[4] K. S. Yee, "Numerical solution of initial value problems involving Maxwell's equations in isotropic media," *IEEE Trans. Antennas Propagat.*, vol. AP-14, pp. 302–307, May 1966.
[5] D. E. Merewether, "Transient currents induced on a metallic body of revolution by an electromagnetic pulse," *IEEE Trans. Electromagn. Compat.*, vol. EMC-13, pp. 41–44, May 1971.
[6] A. Taflove and M. E. Brodwin, "Numerical solution of steady-state electromagnetic scattering problems using the time-dependent Maxwell's equations," *IEEE Trans. Microwave Theory Tech.*, vol. MTT-23, pp. 623–630, Aug. 1975.
[7] A. Taflove, "Application of the finite-difference time-domain method to sinusoidal steady-state electromagnetic-penetration problems," *IEEE Trans. Electromagn. Compat.*, vol. EMC-22, pp. 191–202, Aug. 1980.
[8] R. Holland, L. Simpson, and K. S. Kunz, "Finite-difference analysis of EMP coupling to lossy dielectric structures," *IEEE Trans. Electromagn. Compat.*, vol. EMC-22, pp. 203–209, Aug. 1980.
[9] A. Taflove and K. R. Umashankar, "Finite-difference time-domain (FD–TD) modeling of electromagnetic wave scattering and interaction problems," *IEEE Trans. Antennas Propagat. Soc. Newsletter*, pp. 5–20, Apr. 1988.
[10] J. A. Stratton, *Electromagnetic Theory*. New York: McGraw-Hill, 1941.
[11] E. Isaacson and H. B. Keller, *Analysis of Numerical Methods*. New York: Wiley, 1967.
[12] D. C. Chang, "On the electrically thick monopole Part I—Theoretical solution," *IEEE Trans. Antennas Propagat.*, vol. AP-16, pp. 58–64, Jan. 1968.
[13] C.-Y. Ting, "Theoretical study of a cylindrical antenna with a hemispherical cap," *IEEE Trans. Antennas Propagat.*, vol. AP-17, pp. 716–721, Nov. 1969.
[14] W. Franz, "Zur Formulierung des Huygensschen Prinzips," *Z. Naturforsch*, vol. 3a, pp. 500–506, 1948.
[15] C.-T. Tai, "Kirchoff theory: Scalar, vector, or dyadic," *IEEE Trans. Antennas Propagat.*, vol. AP-20, pp. 114–115, Jan. 1972.
[16] L. J. Cooper, "Monopole antennas on electrically thick conducting cylinders," Ph.D. dissertation, Harvard Univ., Cambridge, MA, Mar. 1975.
[17] S. A. Schelkunoff, *Advanced Antenna Theory*. New York: Wiley, 1952.
[18] R. W. P. King, *The Theory of Linear Antenna*. Cambridge, MA: Harvard Univ. Press, 1956, ch. VIII.

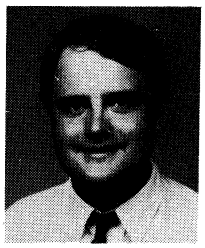

James G. Maloney (S'85) was born in New York, NY, on August 17, 1965. He received the B.E.E. degree from the Georgia Institute of Technology, Atlanta, GA, in 1987.

From 1987 to 1989, he was a Graduate Research and Teaching Assistant in the School of Electrical Engineering at the Georgia Institute of Technology, where he is currently a DuPont and J.S.E.P. Fellow.

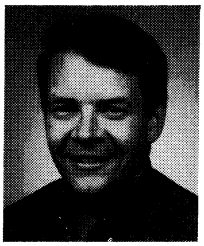

Glenn S. Smith (S'65–M'72–SM'80–F'86) was born in Salem, MA, on June 1, 1945. He received the B.S.E.E. degree from Tufts University, Medford, MA, in 1967 and the S.M. and Ph.D. degrees in applied physics from Harvard University, Cambridge, MA, in 1968 and 1972, respectively.

From 1972 to 1975 he served as a Postdoctoral Research Fellow at Harvard University and also as a part-time Research Associate and Instructor at Northeastern University, Boston, MA. In 1975, he joined the faculty of the Georgia Institute of Technology, Atlanta, GA, where he is currently Reagents' Professor of Electrical Engineering.

Dr. Smith is co-author of the book, *Antennas in Matter: Fundamentals, Theory and Applications*.

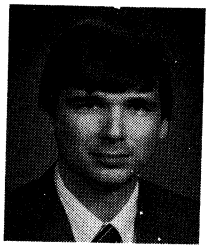

Waymond R. Scott, Jr. (S'81–M'82–M'82–M'85) was born in Calhoun, GA, on April 6, 1958. He received the B.E.E., M.S.E.E., and Ph.D. degrees from the Georgia Institute of Technology, Atlanta, in 1980, 1982 and 1985, respectively.

From 1979 to 1980, he was a Student Assistant and Graduate Research Assistant at the Georgia Tech Research Institute, and from 1980 to 1985, he was a Graduate Research Assistant in the School of Electrical Engineering at the Georgia Institute of Technology, where he is currently an Assistant Professor of Electrical Engineering.